HIC1 and miR-23~27~24 clusters form a double-negative feedback loop in breast cancer

Yanbo Wang[1,*], Hongwei Liang[1,*], Geyu Zhou[1,*], Xiuting Hu[1,*], Zhengya Liu[1], Fangfang Jin[1], Mengchao Yu[1], Jianfeng Sang[2], Yong Zhou[3], Zheng Fu[1], Chen-Yu Zhang[1], Weijie Zhang[4,#] , Ke Zen[1,#], Xi Chen[1,#]

Summary

The Supplementary information includes Supplementary Methods (information of mathematical modeling), Supplementary Tables and Supplementary Figures.

Supplementary Methods

Mathematical modeling

Cancers of the breast and other tissues arise from the disruption of the normal cell signaling network which controls the cell proliferation or apoptosis. We found that the positive feedback loop between the miR-23~27~24 cluster and HIC1 may play an important role in breast cancer progression. Positive feedback loop is a significant motif in the signaling network, because it is able to generate bistability and switch-like behavior (1). Mathematical model is a tool to investigate the dynamic property of this positive feedback loop and to theoretically explore its impact on tumorigenesis (2). Besides, by comparing the theoretical and experimental results, we could have a more intuitive and systematic understanding of this positive feedback loop quantitatively.

Model formation

Figure 6A summarizes the model with 2 components representing the protein HIC1 and the miR-23~27~24 cluster. Here we chose miR-24 as the representative of the cluster for modeling work. Other miRNAs in the cluster could be modeled in a similar manner. The dynamics of the respective concentrations of HIC1 **p** and miR-24 **m** are described by equation (1) and (2):

$$dp/dt = k_1 / (1 + k_2 m) - \gamma p \quad \textbf{(1)}$$

$$dm/dt = k_3 / (1 + k_4 p^2) - \delta m \quad \textbf{(2)}$$

The rate of synthesis of HIC1 is indicated by the first term on the right-hand side of equation (1), where k_1 represents constitutive protein expression and the denominator $(1 + k_2 m)$ represents miRNA-dependent downregulation of HIC1 expression. The parameter k_2 is the inverse of the miRNA concentration required for half-maximum repression of HIC1 expression. The repression of HIC1 by miR-24 is summarized in equation (2). The parameter k_3 is a lumped parameter that describes the net effect of RNA polymerase binding, open-complex formation, transcript elongation and transcript termination (3). The rate of repression-of HIC1 synthesis by expression of miR-24-is determined by the term $(1 + k_4 p^2)$ in the denominator. The cooperativity described by the Hill exponent 2 can arise from the cooperative binding of HIC1 to two sites in the promoter region of miR-24, a possibility that is supported by the CHIP data (Fig. 4B) and by data in the literature (4). The square root of k_4 is the inverse of the HIC1 concentration required for half-maximum repression of miR-24 expression.

Solving for steady states of the system

The steady states of the system described in equation (1) and equation (2) are determined by setting the time derivatives of **p** and **m** to 0. After eliminating **m** in the equations, the following cubic polynomial is obtained; the non-negative roots of this polynomial give the steady state of **p**.

$$c_3p^3 + c_2p^2 + c_1p + c_0 = 0 \quad \textbf{(3)}$$

where

$$c_3 = \gamma\delta k_4$$

$$c_2 = -k_1k_4\delta$$

$$c_1 = k_2k_3\gamma + \gamma\delta$$

$$c_0 = -k_1\delta$$

The steady state of **m** is given by

$$m = k_3 / \delta(1 + k_4p^2) \quad \textbf{(4)}$$

According to equation (4), the steady states of **p** and **m** increase or decrease in the opposite direction, which agrees with the experimental results.

Parameter values and numerical solution of the equation

To obtain the degradation rate of HIC1, we compared the degradation rate of HIC1 with that of luciferase according to experimental results (Fig. 3F and 3G). Because previous literature has reported the degradation rate of luciferase (5), we normalized and estimated that the degradation rate of HIC1 (γ) is approximately 0.44 h^{-1}.

According to the literature, the degradation rate of miRNA (δ) is typically approximately 0.02 h^{-1} (6, 7); note that this is reasonable considering that miRNA is generally more stable than protein. The rate of synthesis of HIC1 (k_1) is in the range of 0 to 0.1 μM/h, whereas the synthesis rate of miR-24 is approximately 0.002 μM/h. Based on the experimental results, we estimated that the parameters k_2 and k_4 are approximately 1×10^2 μM^{-1} and 3×10^3 μM^{-2}, respectively. The numerical solution was obtained using the Matlab roots function. The non-negative roots were selected and plotted on the bifurcation diagram. For simulation of epigenetic downregulation, the rate of synthesis of HIC1 was chosen to range from 0.06 to 0.03 μM/h, wherease the rate of synthesis of miR-24 was chosen to range from 0 to 0.003 μM/h to mimic the in vitro transfection assay.

The simulation results were converted to relative levels for illustrative purposes. The concentration of HIC1 was assumed to be approximately 0.05-0.08 μM under normal conditions, similar to the concentration of another tumor suppressor, p53 (8). The concentrations of miRNAs have been normalized to that of U6 snRNA. Typically, the copy number of U6 snRNA is 10^5 molecules/cell (BNID 101302 in Bionumbers database (9)); this concentration equals 0.17 μM (1 μM = 6×10^5 molecules/cell, derived from a supplementary file in the literature (10)). Thus, the concentration of miR-24 under normal conditions is approximately 0.012-0.015 μM (approximately 1/10 of U6 snRNA on average derived from qRT-PCR). Based on these calculations, the simulation results could easily be converted into relative levels divided by the

concentration of HIC1 and miR-24 under normal conditions. After conversion, the relative level of HIC1 and miR-24 under normal conditions was approximately 1, indicating the accuracy of calculations and model predictions. Then the experimental results were plotted for further analysis as described in the main text. Notice that only small portion of miRNAs measured by qRT-PCR will be loaded in the functional RISC complex after transient transfection of mimic-miRs, suggesting the necessary of adjusting the experimentally measured miR-24 level to much lower and functional one (11) (5% in this case). Two rules were applied when optimizing and plotting the results: (i) each samples plotted in different figures (Fig. 6B and 6C, Fig. 6D and 6E) were paired and had the same synthesis rate (x-axis position); (ii) the theoretical prediction should generally match the experimental results.

References:

1. Ferrell JE, Jr. Self-perpetuating states in signal transduction: positive feedback, double-negative feedback and bistability. Current opinion in cell biology. 2002;14:140-8.
2. Tyson JJ, Baumann WT, Chen C, Verdugo A, Tavassoly I, Wang Y, et al. Dynamic modelling of oestrogen signalling and cell fate in breast cancer cells. Nature reviews Cancer. 2011;11:523-32.
3. Gardner TS, Cantor CR, Collins JJ. Construction of a genetic toggle switch in Escherichia coli. Nature. 2000;403:339-42.
4. Pinte S, Stankovic-Valentin N, Deltour S, Rood BR, Guerardel C, Leprince D. The tumor suppressor gene HIC1 (hypermethylated in cancer 1) is a sequence-specific transcriptional repressor: definition of its consensus binding sequence and analysis of its DNA binding and repressive properties. The Journal of biological chemistry. 2004;279:38313-24.
5. Bartlett DW, Davis ME. Insights into the kinetics of siRNA-mediated gene silencing from live-cell and live-animal bioluminescent imaging. Nucleic Acids Res. 2006;34:322-33.
6. Johnston RJ, Jr., Chang S, Etchberger JF, Ortiz CO, Hobert O. MicroRNAs acting in a double-negative feedback loop to control a neuronal cell fate decision. Proc Natl Acad Sci U S A. 2005;102:12449-54.
7. Aguda BD, Kim Y, Piper-Hunter MG, Friedman A, Marsh CB. MicroRNA regulation of a cancer network: consequences of the feedback loops involving miR-17-92, E2F, and Myc. Proc Natl Acad Sci U S A. 2008;105:19678-83.

8. Zhou CH, Zhang XP, Liu F, Wang W. Involvement of miR-605 and miR-34a in the DNA damage response promotes apoptosis induction. Biophys J. 2014;106:1792-800.
9. Milo R, Jorgensen P, Moran U, Weber G, Springer M. BioNumbers--the database of key numbers in molecular and cell biology. Nucleic Acids Res. 2010;38:D750-3.
10. Bhalla US, Iyengar R. Emergent properties of networks of biological signaling pathways. Science. 1999;283:381-7.
11. Thomson DW, Bracken CP, Szubert JM, Goodall GJ. On measuring miRNAs after transient transfection of mimics or antisense inhibitors. PLoS One. 2013;8:e55214.

Supplementary Tables

Supplementary Table S1. Patients' Characteristics.

Patients' characteristics					
Case No.	Clinical History	Gender	Age (years)	TNM Stage	Hormone Receptor
BC #1	IDC	Female	44	III	ER-, PR-, HER2/neu+
BC #2	IDC	Female	60	II	ER/PR+, HER2/neu+
BC #3	IDC	Female	47	II	ER/PR+, HER2/neu+
BC #4	IDC	Female	49	II	ER/PR+, HER2/neu+
BC #5	IDC	Female	41	II	ER/PR+, HER2/neu+
BC #6	IDC	Female	39	III	ER/PR+, HER2/neu-
BC #7	IDC	Female	47	III	ER+, PR-, HER2/neu+
BC #8	IMPC	Female	48		
BC #9	IDC	Female	44	III	ER/PR-, HER2/neu-
BC #10	IDC	Female	57	II	ER/PR+, HER2/neu+
BC #11	IDC	Female	54	I	ER/PR+, HER2/neu+
BC #12	IDC	Female	41	II	ER/PR+, HER2/neu-
BC #13	IDC	Female	44	II	ER-, PR-, HER2/neu+
BC #14	IMPC	Female	48		
BC #15	IDC	Female	56	III	ER/PR+, HER2/neu+
BC #16	IDC	Female	58	II	ER/PR+, HER2/neu+
BC #17	IDC	Female	60	II- III	ER/PR+, HER2/neu+
BC #18	IDC	Female	56	II	ER+, PR-, HER2/neu-
BC #19	IDC	Female	58	III	ER-, PR-, HER2/neu+
BC #20	IDC	Female	66	II- III	ER/PR+, HER2/neu+
BC #21	IDC	Female	62	II- III	ER/PR-, HER2/neu-
BC #22	IDC	Female	42	II	
BC #23	IDC	Female	47	II	ER+, PR-, HER2/neu-
BC #24	IDC	Female	43	II	
BC #25	IDC	Female	46	II- III	ER/PR+, HER2/neu-

Supplementary Figures and Legends

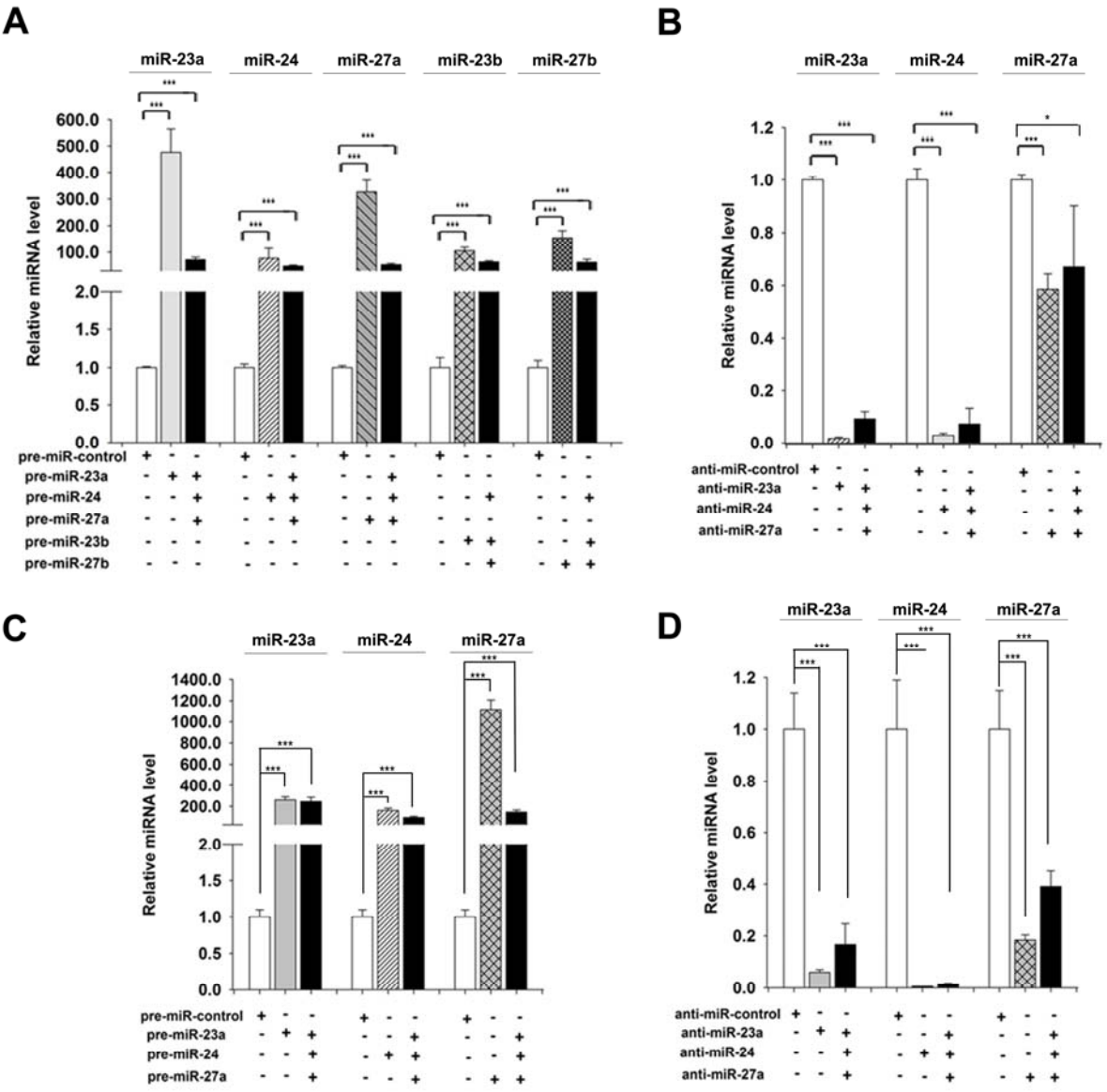

Supplementary Figure S1. The cellular levels of miRNAs after transfecting with pre-miRNA mimics or antisense miRNAs. (A-D) Quantitative RT-PCR analysis of the levels of miR-23a/b, miR-24 and miR-27a/b in MCF-7 (A and B) and MDA-MB-231 (C and D) cells treated with pre-miR-control, pre-miR-23a/b, pre-miR-24, pre-miR-27a/b or a mixture of these pre-miRs, or with anti-miR-control, anti-miR-23a, anti-miR-24, anti-miR-27a or a mixture of these anti-miRs.

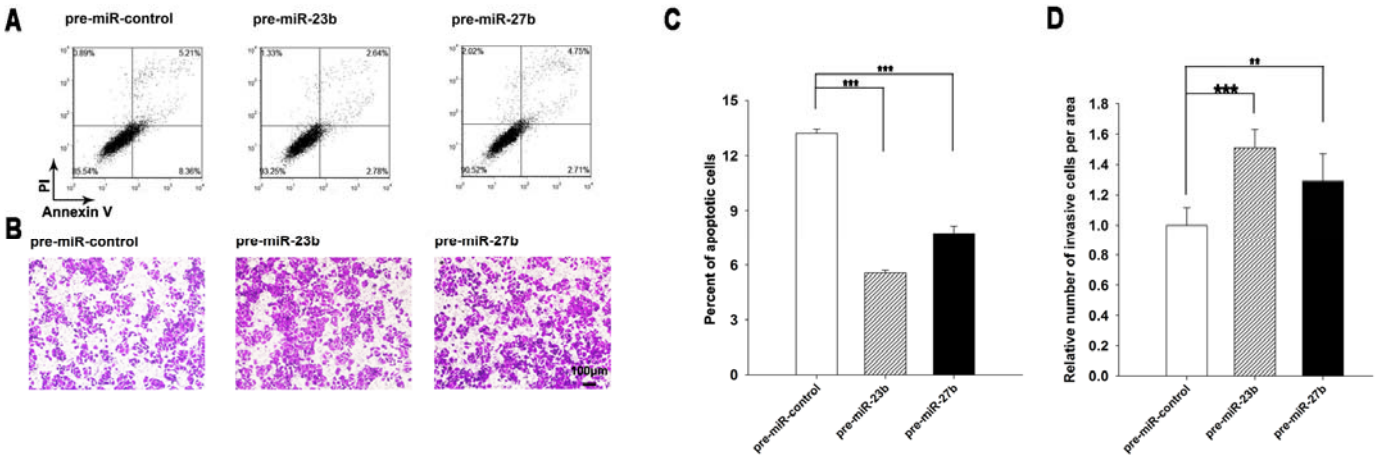

Supplementary Figure S2. The effects of miR-23b and miR-27b on the apoptosis and invasion of MCF-7 cells. (A and C) Analysis of apoptosis in MCF-7 cells treated with pre-miR-control, pre-miR-23b or pre-miR-27b. The total apoptotic cells were counted as the sum of early apoptotic (PI^- AV^+) and late apoptotic (PI^+ AV^+) cells. A: representative image; C: quantitative analysis. **(B and D)** Transwell analysis of invaded MCF-7 cells treated with pre-miR-control, pre-miR-23b or pre-miR-27b. B: representative image; D: quantitative analysis. ** $P < 0.01$; *** $P < 0.001$.

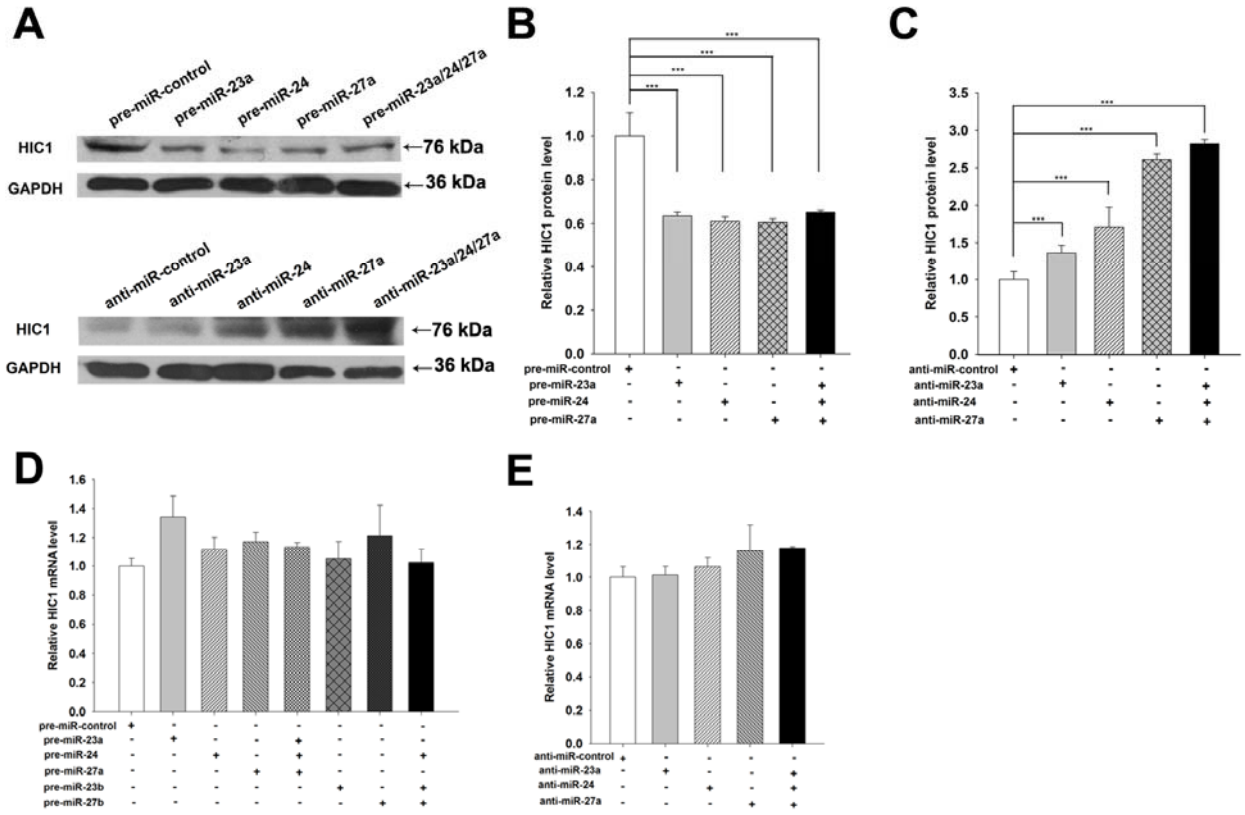

Supplementary Figure S3. Validation of HIC1 as a direct target of miR-23~27~24 clusters in MDA-MB-231 cells. (A-C) Western blot analysis of the expression levels of HIC1 protein in MDA-MB-231 cells treated with pre-miR-control, pre-miR-23a, pre-miR-24, pre-miR-27a or a mixture of these pre-miRs, or with anti-miR-control, anti-miR-23a, anti-miR-24, anti-miR-27a or a mixture of these anti-miRs. A: representative image; B and C: quantitative analysis. **(D and E)** Quantitative RT-PCR analysis of the expression levels of HIC1 mRNA in MCF-7 cells treated with pre-miR-control, pre-miR-23a/b, pre-miR-24, pre-miR-27a/b or a mixture of these pre-miRs, or with anti-miR-control, anti-miR-23a, anti-miR-24, anti-miR-27a or a mixture of these anti-miRs. *** $P < 0.001$.

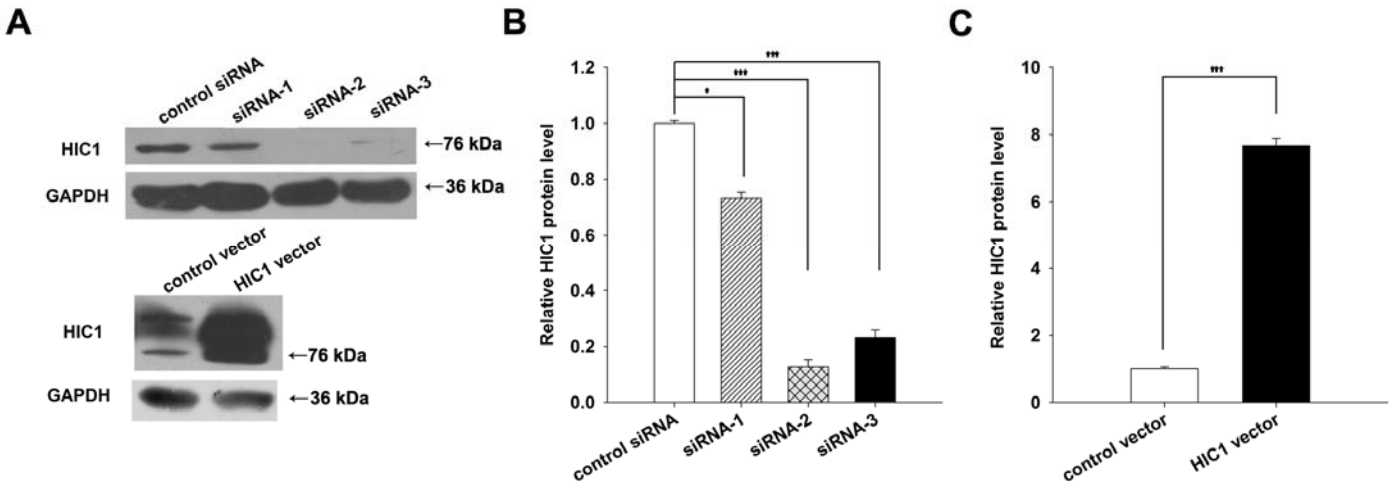

Supplementary Figure S4. Silencing of HIC1 by siRNA and overexpression of HIC1 by a vector. (A-C) Western blotting analysis of HIC1 protein levels in MCF-7 cells treated with control siRNA, HIC1 siRNA-1, HIC1 siRNA-2, HIC1 siRNA-3, or with control vector or HIC1 vector. A: representative image; B and C: quantitative analysis. * $P < 0.05$; *** $P < 0.001$.

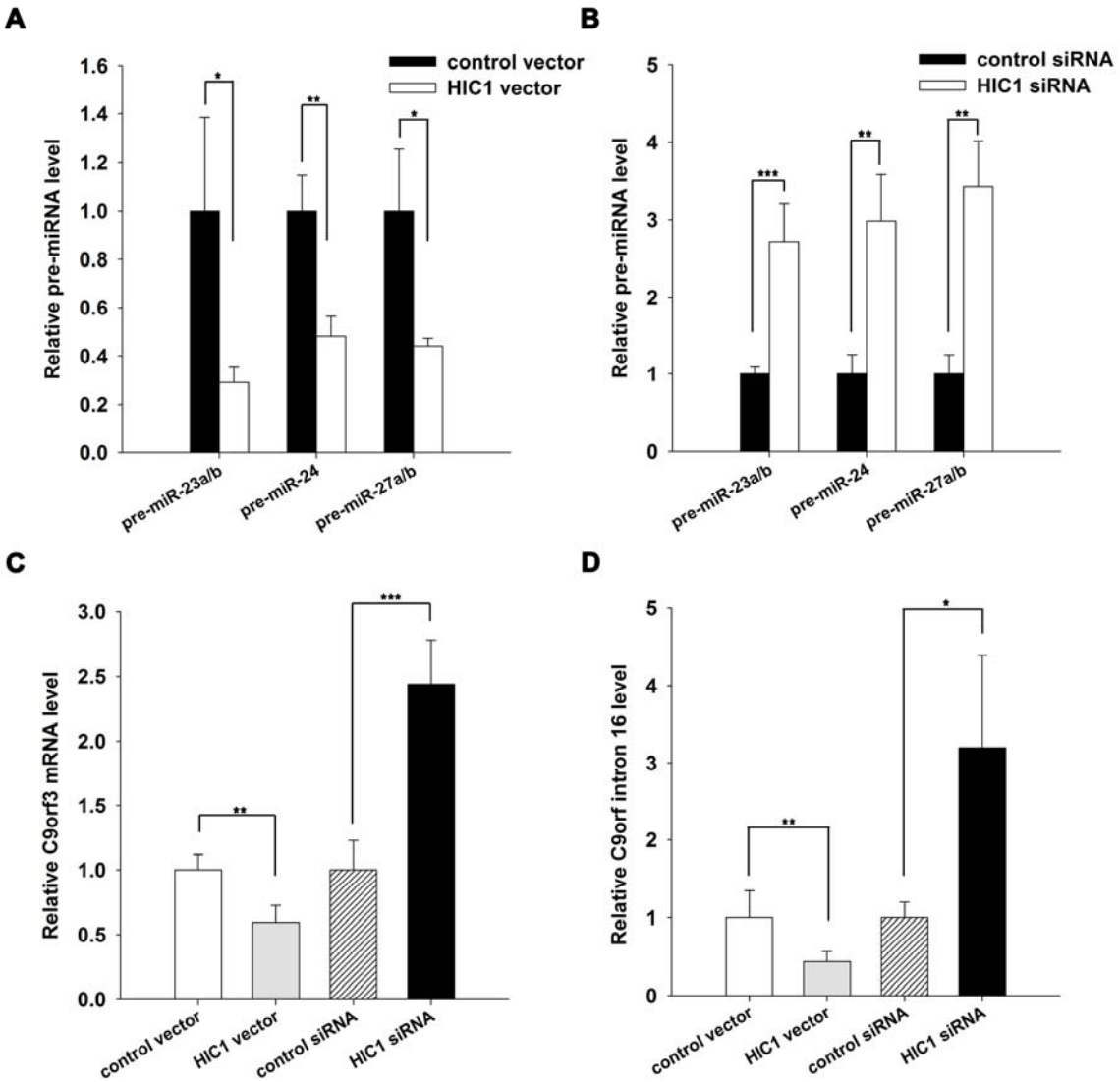

Supplementary Figure S5. HIC1 directly inhibits miR-23~27~24 clusters in transcriptional level. (A) Quantitative RT-PCR showing that ectopic expression of HIC1 downregulates the expression of pre-miR-23, pre-miR-24 and pre-miR-27 in MCF-7 cells. **(B)** Quantitative RT-PCR showing that knockdown of HIC1 by siRNA upregulates the expression of pre-miR-23, pre-miR-24 and pre-miR-27 in MCF-7 cells. **(C)** Quantitative RT-PCR showing that ectopic expression of HIC1 downregulates the expression of C9orf3 mRNA and the sixteenth intron of C9orf3 in MCF-7 cells. **(D)** Quantitative RT-PCR showing that knockdown of HIC1 by siRNA upregulates the expression of C9orf3 mRNA and the sixteenth intron of C9orf3 in MCF-7 cells. * $P < 0.05$; ** $P < 0.01$; *** $P < 0.001$.

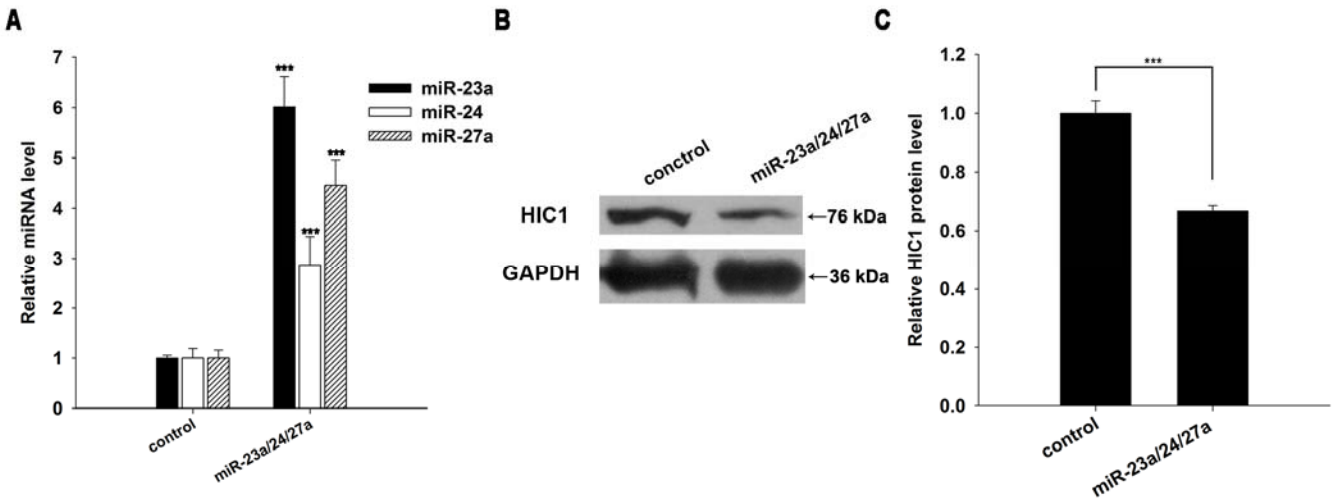

Supplementary Figure S6. Downregulation of HIC1 by a lentiviral miR-23a/24/27a expression vector in MCF-7 cells. (A) Quantitative RT-PCR analysis of miR-23a, miR-24 and miR-27a levels in MCF-7 cells infected with a lentiviral miR-23a/24/27a expression vector. **(B and C)** Western blotting analysis of HIC1 protein levels in MCF-7 cells infected with a lentiviral miR-23a/24/27a expression vector. B: representative image; C: quantitative analysis. *** $P < 0.001$.